

**APPENDIX C**

**SUMMARY OF RECENT INFORMATION RELEVANT TO  
NEAR-FIELD ENVIRONMENT PROCESS MODEL**

INTENTIONALLY LEFT BLANK

## **SUMMARY OF RECENT INFORMATION RELEVANT TO NEAR-FIELD ENVIRONMENT PROCESS MODEL**

### **1. INTRODUCTION**

This white paper contains a summary of recent test results and other additional information that are relevant to the near-field environment process model used to support the *Yucca Mountain Science and Engineering Report* (YMS&ER) (DOE 2001a) and the *Yucca Mountain Preliminary Site Suitability Evaluation* (YMPSSE) (DOE 2001b). The U.S. Department of Energy (DOE) released these two documents for public review in May and August, respectively, of this year.

The white paper focuses on the results of those field and laboratory tests and other additional information that became available after the near-field environment process model was completed to support the preparation of the YMS&ER and the YMPSSE. The summary of this recent information is being used to conduct an impact review, in accordance with AP-2.14Q, *Review of Technical Products and Data*, to determine if this additional information has any impact on the technical analyses supporting the YMS&ER and the YMPSSE. The documentation of the additional information in this white paper is an interim step and primarily used to support this impact review. This information is expected to be formally documented in subsequent DOE technical reports, as appropriate.

To assist in the impact review, this white paper briefly describes the near-field environment process model that was used to support the YMS&ER and the YMPSSE, provides a summary of the recent test results and other additional information, and discusses the potential implications of this more recent information on our understanding of the near-field environment process model.

### **2. SUMMARY DESCRIPTION OF THE NEAR-FIELD ENVIRONMENT PROCESS MODEL**

This section provides a brief description of the process models that were used to support the YMS&ER (DOE 2001a) and the YMPSSE (DOE 2001b). Decay heat generated by nuclear wastes will have a number of effects on the host rock units (CRWMS M&O 2000a, Section 1.1). The most direct effect is on the movement of water through various thermal-hydrologic mechanisms like rock dryout and vapor flow. Another effect is on rock–water interaction (chemical processes), occurring as a result of the flux of water, vapor, and dissolved constituents and because the elevated temperatures may enhance the reactivity of the various phases involved. The heat-driven deformation of the rock mass (mechanical processes) may also affect the movement of water by affecting the rock permeability. The conceptual basis of each of these processes is discussed briefly below

## **2.1 THERMAL-HYDROLOGIC EFFECTS**

Thermal-hydrologic effects as a result of decay heat will be important in both the preclosure and postclosure periods. During preclosure, forced ventilation will remove 70 percent of the heat in the first 50 years (DOE 2001a, Section 4.2.2.1.1), with the remaining heat transferred to the host rock by radiation, conduction, and convection. The major effects of decay heat on water movement would occur after closure (CRWMS M&O 2000b, Section 6.11.4). Initially, heat will be transported radially away from the drifts by conduction through the rock and by advection of air and water vapor through fractures. A portion of the heat will be transferred locally by water vapor that condenses in cooler rock farther away. If the heat flux is high enough, rock near the drifts will be heated to the boiling point of water (nominally 96°C [205°F] at the elevation of the repository) and then to higher temperatures after most of the water in the rock matrix of this region has evaporated. The region within which substantially all the water has evaporated is called the dryout zone. Surrounding the dryout zone, a heat pipe zone characterized by two-phase conditions would form within which the temperature is essentially constant at the boiling point. The heat pipe zone would be surrounded by a condensation zone of increased water saturation and temperature below the boiling point. After closure, these regions will first expand, then contract as the heat output diminishes over time, this sequence of heating and cooling of a repository being referred to as the thermal pulse.

## **2.2 THERMAL-HYDROLOGIC-CHEMICAL EFFECTS**

The temperature changes and the movement of water caused by the radioactive decay heat will also drive chemical changes in the near-field environment (thermal-hydrologic-chemical effects). Changes may result from the increase in temperature because both mineral solubilities and reaction rates are known to be strong functions of temperature. More important than the temperature effects alone, however, is the direct effect of the thermal-hydrologic processes on chemical reactions surrounding nuclear waste repositories. All species will become more concentrated in the dryout zone due to evaporation, potentially leading to precipitation of various mineral phases, especially salts. These salts may be redissolved as the thermal system contracts, and the local rock undergoes rewetting (BSC 2001a). The local mass of water that can be evaporated, however, is relatively small, so relatively small amounts of mineral deposition are expected from this mechanism. More abundant mineral deposition is possible within the heat pipe zone where the repeated flux of liquid water in to, and evaporation from, the zone may produce substantial amounts of secondary mineralization. In addition to the deposition of salts, formation of silicate mineral phases may alter the porosity and permeability of the fracture network, thus modifying the local thermal-hydrologic regime. Mineral alteration may also occur in the subboiling condensation zone where high CO<sub>2</sub> in the gas phase may result in low pH values in the aqueous phase. These low pH waters could be capable of aggressive reaction with primary minerals in the local host rock. Current analyses of these potential thermal-hydrologic-chemical effects indicate that there should only be minor amounts of mineral precipitation in fractures evaluated in regions as small as 20 cm (8 in.). This mineral alteration corresponds to a less than 10 percent decrease in fracture permeability in the system (BSC 2001a).

## 2.3 THERMAL-HYDROLOGIC-MECHANICAL EFFECTS

The *Near-Field Environment Process Model Report* (CRWMS M&O 2000a) concludes that the primary effect of the uncertainty in thermal-hydrologic-mechanical responses is a potential modification of the fracture permeability, with an increase of up to one order of magnitude in rock permeability possible. The stress field in the rock mass surrounding emplacement drifts would be altered by excavation of drifts and by the heating/cooling cycle associated with emplacement of radioactive waste. The direction and magnitude of principal stresses will change because of thermal loading and then will return to near-ambient values during cooldown. The return to ambient conditions will not be comprehensive because of deformation that would occur as a result of stress redistribution during this cycle. The magnitude of changes in hydrologic properties should be limited (CRWMS M&O 2000a, Section 3.5). The fractures in the Yucca Mountain tuffs are expected to deform as stress conditions evolve. Because the permeability of the tuff is almost exclusively in the fractures, large changes in rock permeability may result from fracture deformation.

### 2.3.1 Summary of Thermal Testing

A series of tests have been designed and conducted in order to build confidence in both the conceptual basis of the process models and the parameters used as inputs to those models (CRWMS M&O 2000a). These tests have been carried out at a variety of scales, ranging from core-sized laboratory tests, to meter-scale bench tests, to small and large scale in situ field tests. Most important of these are the Large Block Test, the Single Heater Test, and the Drift Scale Test.

To construct the Large Block Test, a  $3 \times 3 \times 4.5$  m ( $10 \times 10 \times 15$  ft) block of the middle nonlithophysal member of the Topopah Spring Tuff was isolated as a column. Fractures were mapped on five exposed surfaces and in boreholes. The exposed surfaces were later insulated thermally and covered to prevent water flow. Five heaters were installed in the block to form a horizontal heater plane at about 2.743 m (9 ft) from the top. Instruments were installed in boreholes to measure temperature, gas pressure, relative humidity, moisture content (using neutron logging), and deformations. In addition, instruments installed on the block-surface include electrodes for electrical-resistance tomography (ERT), fracture gauges, and resistance-temperature devices (RTD) to monitor the near-surface temperature gradients. Deformations within the block were measured by multiple-point borehole extensometers (MPBXs) for bulk displacements within the block (CRWMS M&O 2000a).

The Single Heater test is described in *Single Heater Test Final Report* (CRWMS M&O 1999) and in the *Near Field Environment Process Model Report* (CRWMS M&O 2000a, Section 3.6.1.2). The primary purpose of the Single Heater Test was to investigate the thermal-mechanical responses of the rock mass caused by heating from a single heater in a borehole. Temperature was measured with thermocouples and with resistance thermometers. Rock mass displacement was measured with MPBX, while ERT was used to monitor the moisture content of the rock.

Both the Large Block Test and the Single Heater Test were completed by the time of the publication of the *Yucca Mountain Science and Engineering Report* (DOE 2001a) and the *Yucca*

*Mountain Preliminary Site Suitability Evaluation* (DOE 2001b). The Drift Scale Test, however, is ongoing as of October 2001, with two months left in the a four-year heating period, which will be followed by a four-year cooling period. The heated drift of the Drift Scale Test is 5 m (16 ft) in diameter, 47.5 m (156 ft) in length, and nominally isolated from the access drift by an insulated thermal bulkhead. Nine floor/canister heaters in the heated drift and 50 wing heaters (in horizontal boreholes perpendicular to the drift) initially generated approximately 190 kW of power over a 1,500 m<sup>2</sup> (1600 ft<sup>2</sup>) area. The conceptual understanding gained from the Drift Scale Test is summarized in the YMS&ER (DOE 2001a) and the YMPSSSE (DOE 2001b), while a description of actual testing results is available in summary form in the *Near Field Environment Process Model Report* (CRWMS M&O 2000a) and in detail in the *Thermal Test Progress Report #6* (Williams 2001).

### **3. SUMMARY OF RECENT TEST RESULTS AND OTHER ADDITIONAL INFORMATION**

This section summarizes recent results from the different field or laboratory tests that have provided information relevant to enhancing our understanding of the near-field environment process model. The test and studies that provided this additional information are listed below and discussed in each of the sections that follow:

1. Drift Scale Test
2. Natural analogue studies.

Because of the recent nature of the information provided in this section, much of it is unpublished; therefore, some source references have been provided where appropriate, but others could not be provided. However, this information is currently documented in the principal investigators' scientific notebooks, if applicable, in accordance with the Project's quality assurance procedure AP-SIII.1Q, *Scientific Notebooks*.

#### **3.1 DRIFT SCALE TEST**

The Drift Scale Test is a large-scale, heated field test designed to generate and to observe thermally driven effects on hydrologic, mechanical, and chemical coupled processes in the welded tuff units of the potential repository site at Yucca Mountain (Figure 1). While the evolution of the Drift Scale Test will not mimic the potential repository exactly, the same fundamental processes are expected to occur in both. As the processes taking place in the Drift Scale Test are quantified, they can be used to validate the models developed to describe them. For this reason, DOE has taken the approach that close integration between modeling and measurements is necessary. Numerical models were constructed for the Drift Scale Test and were used to carry out pretest modeling of the results. As the test progresses, data are continuously collected, evaluated, and compared continuously to the model predictions—where necessary, the model(s) are iteratively refined to incorporate insights from the test.

The Drift Scale Test is densely instrumented to record temperatures, rock movement, fluid movement, gas flow, and to sample liquids and gases from the rock mass (Figure 1). Samples of rock are also collected periodically from boreholes to identify and observe mineralogic alteration at various distances from the heated drift.

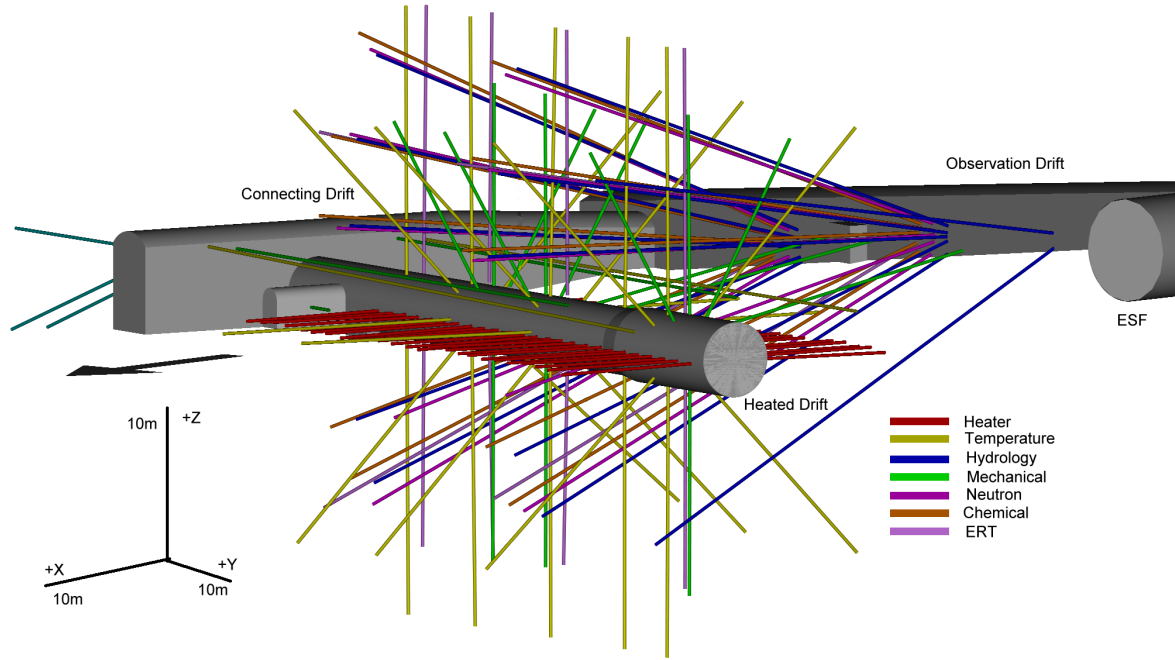


Figure 1. Illustration of the Drift Scale Test, Showing Locations of Various Monitoring Boreholes

### 3.1.1 Thermal Data from the Drift Scale Test Through Mid-October, 2001

As shown in Figure 2, the test, as of mid-October 2001, is about two months from completing its planned four-year heating period. The planned thermal management strategy for the Drift Scale Test includes maintaining the wall temperature in the heated drift at approximately 200°C (392°F). Figure 3 illustrates the temperature distribution on the walls of the heated drift on day 1,396 (October 1, 2001). Figure 3 shows that the temperature on the drift walls is within about 10°C of its target temperature of 200°C (392°F). Figure 2 shows that the drift wall has been very close to its target temperature of 200°C (392°F) since about day 850 (April 3, 2000). The planned power reductions, therefore, have been successful in maintaining the drift wall temperature at the desired level up to the latest period for which data are available.

Coordinate directions in the Drift Scale Test are defined as follows. The Y-coordinate direction is defined as the direction along the axis of the heated drift, with the origin ( $Y = 0$ ) defined by the position of the bulkhead. The X-coordinate direction is in the same horizontal plane as the Y-coordinate, with +x being to the right as one views the drift from the bulkhead. The Z-coordinate direction is the vertical plane, with positive values above the mid-height of the drift.

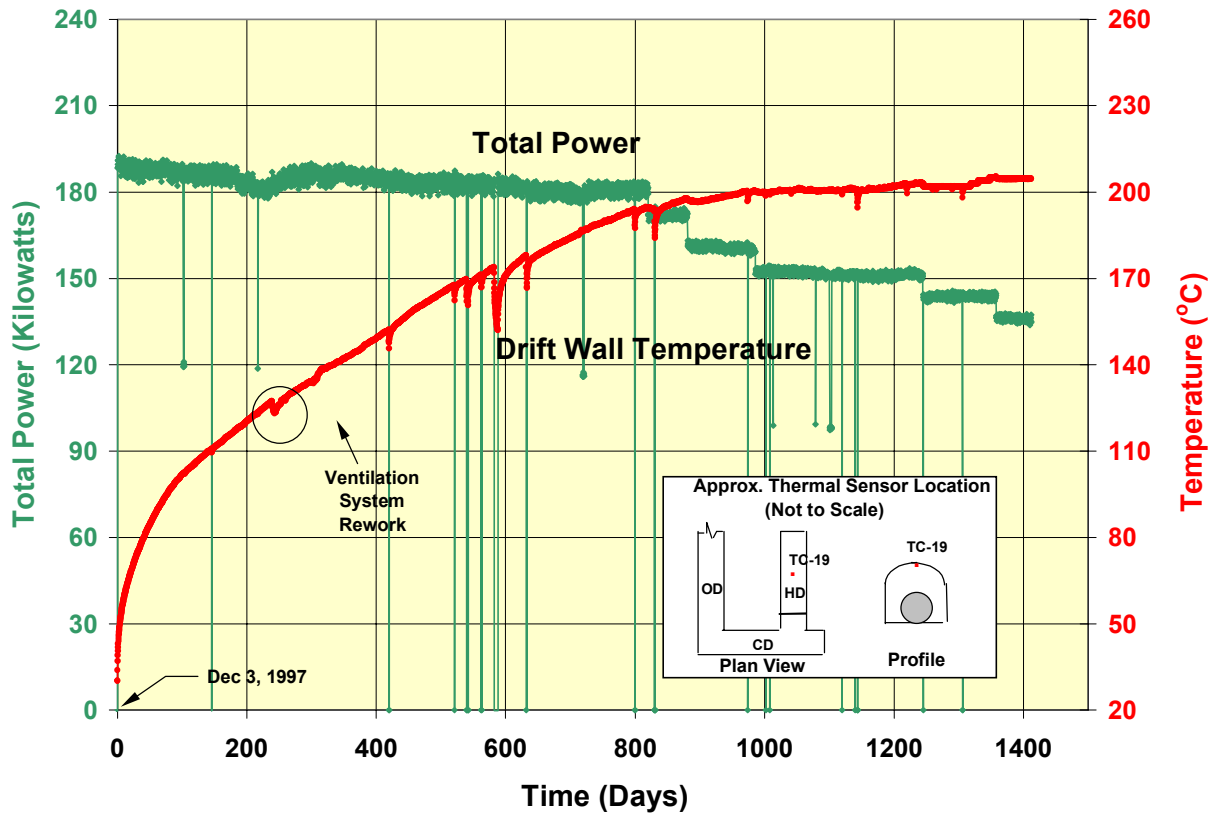


Figure 2. Power and Drift Wall Temperature History for the Drift Scale Test through mid-October, 2001

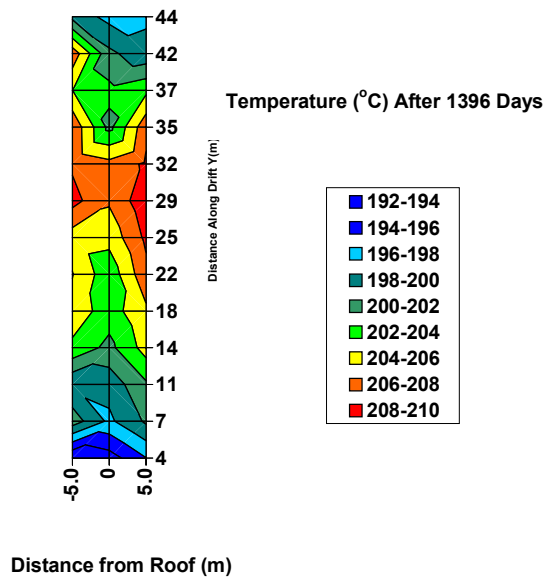


Figure 3. Measured Temperature Distribution on Heated Drift Walls on Day 1,396 (October 1, 2001)

Figure 4 illustrates the temperature as a function of distance along the Y–coordinate direction in borehole 79. This hole is oriented parallel to the Y-coordinate direction at approximately  $X = 9.5$  m (31 ft) and  $Z = 3$  m (10 ft). In Figure 4, the lowest-most curve illustrates the temperatures recorded in the hole just prior to heater activation and subsequent curves portray the temperatures every 90 days thereafter. As is evident from Figure 4, the latest temperature profile (day 1,366, September 2001) is very similar to the profiles recorded earlier. Temperatures continue to rise close to  $Y = 0$  meters, while the gradient in temperature has increased slightly near  $Y = 18$  m (59 ft). The nearly isothermal sections apparent at earlier times close to the boiling point have disappeared, presumably because all of the local water has been vaporized. Another interesting thermal signature is evident in Figure 4 is the temperature behavior near  $Y = 12$  m (39 ft). At subboiling temperatures the rock near this location was substantially warmer than the rock on either side of it. Near the boiling point, the temperature profile was essentially constant, and at temperatures exceeding the boiling point the rock near this location was somewhat cooler than the surrounding rock. A possible explanation for this behavior is the existence of a near vertical fracture at this location. The higher initial temperatures may reflect flow of vapor upwards through the rock, enhancing heating of this location. The lower temperatures that prevailed later may reflect cooler water flowing downward in the fracture toward the heated region. By September 2001 (the last profile), this behavior had disappeared, probably the natural result of the drying front moving far enough away from this suspected fracture. While there has been some change in the temperature profiles of individual boreholes in recent months, the evolution appears to be the natural result of the thermal-hydrologic processes involving water and vapor flow and the dryout of the rock.

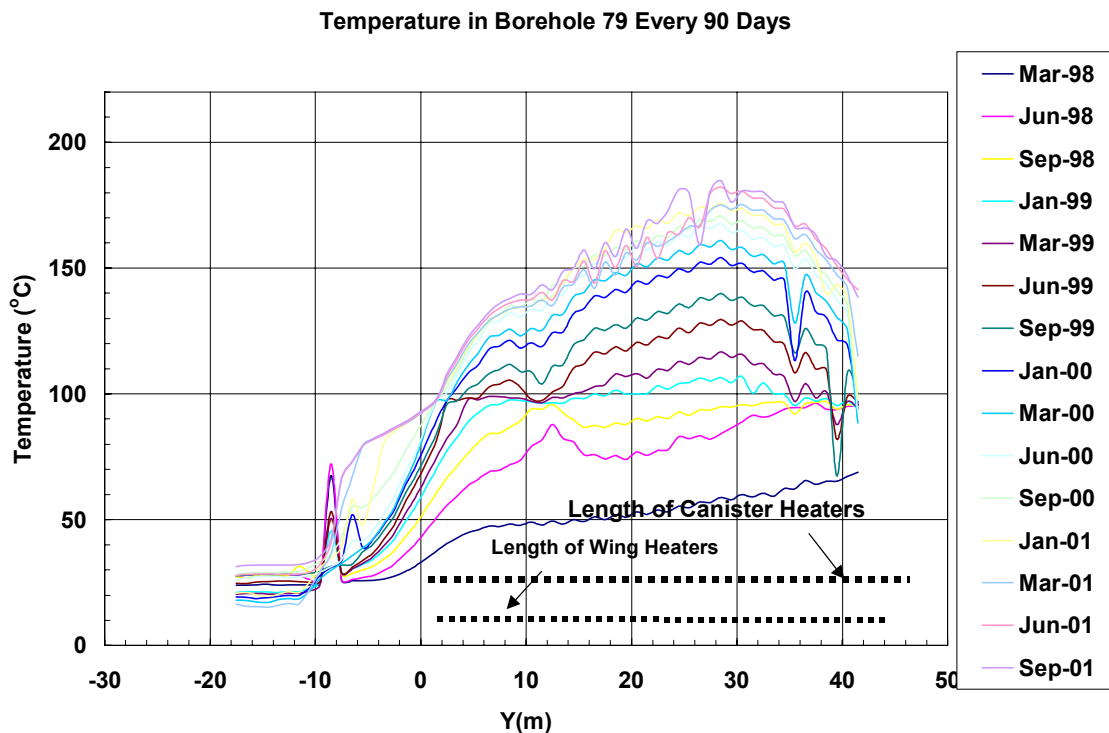


Figure 4. Temperatures in Borehole 79 Every 90 Days

### 3.1.2 Field Thermal Tests—The Effect of Heat on the Flow of Water

The flow of water is one of the most important processes being investigated in the site characterization program at Yucca Mountain, Nevada. Understanding the process of the water movement under the influence of the radioactive decay heat of the nuclear waste will enhance the accuracy of predicting hydrologic and chemical conditions in emplacement drifts and the transport of radioactive nuclides from the emplacement drifts to the accessible environment. The conceptual model of the effect of the heat on the movement of water is that the heat evaporates the pore water into vapor; the water vapor flows from the matrix into near-by fractures following pressure gradients. The vapor will take the paths of least resistance by flowing in fractures. The water vapor will condense into liquid water in the fractures at the cooler locations. The condensate may be imbibed into the matrix or flows along fractures under the influence of gravity. Depending on the combined effects of gravity and fracture orientation, the condensate may flow away from or toward the heat source. The condensate that is imbibed into the matrix will increase the matrix saturation, which will affect the thermal-hydrologic process during the later period of the heating phase. The condensate that flows back toward the heat source may be evaporated/boiled again, and another cycle of vapor flow, condensation, and condensate flow will start again. The condensate that is drains away from the heat source may not participate in later phases of the thermal-hydrologic processes, depending on the distance it migrates.

In the Drift Scale Test, the heat-driven water flow is monitored by various means. The change of water saturation in the rock mass caused by the water movement is measured by geophysical methods, such as neutron logging, ground-penetrating radar (GPR), and ERT. Temperature is sensitive to the flow of water as both a vapor and a liquid. Air permeability in fractures is used to infer the variation of water content in fractures, assuming that changes in fracture permeability are not the result of other processes (e.g., thermal-mechanical or thermal-chemical).

#### 3.1.2.1 Temperature as a Diagnostic of Water Movement

In the Drift Scale Test, temperature is measured in the heated drift, in the rock mass in both RTD holes, and in the rock mass in MPBX holes. Because the RTD holes are sealed, the temperatures measured in them are the most representative of the actual temperatures in the rock mass. The temperatures measured in the RTD holes are used in this discussion of the heat-driven water movements

Figure 5 shows the temperature measured at a number of resistance temperature devices as a function of days since the start of heating in borehole 144, which is at 12 m (39 ft) from the bulkhead and is oriented 45° from the Access Observation Drift. This figure is used as an example to illustrate the effects of heat transfer and moisture movement on the temperature. The curve RTD-1 in Figure 5 shows the typical temperature-time curve of heat conduction in a partially saturated medium. The temperature rises quickly at first due to a large thermal gradient between the heat source and RTD-1. With time, however, the rate of increase in the temperature decreases due to lessening of the thermal gradients and because of the cooling effect resulting from the evaporation of water.

ESF-HD-144

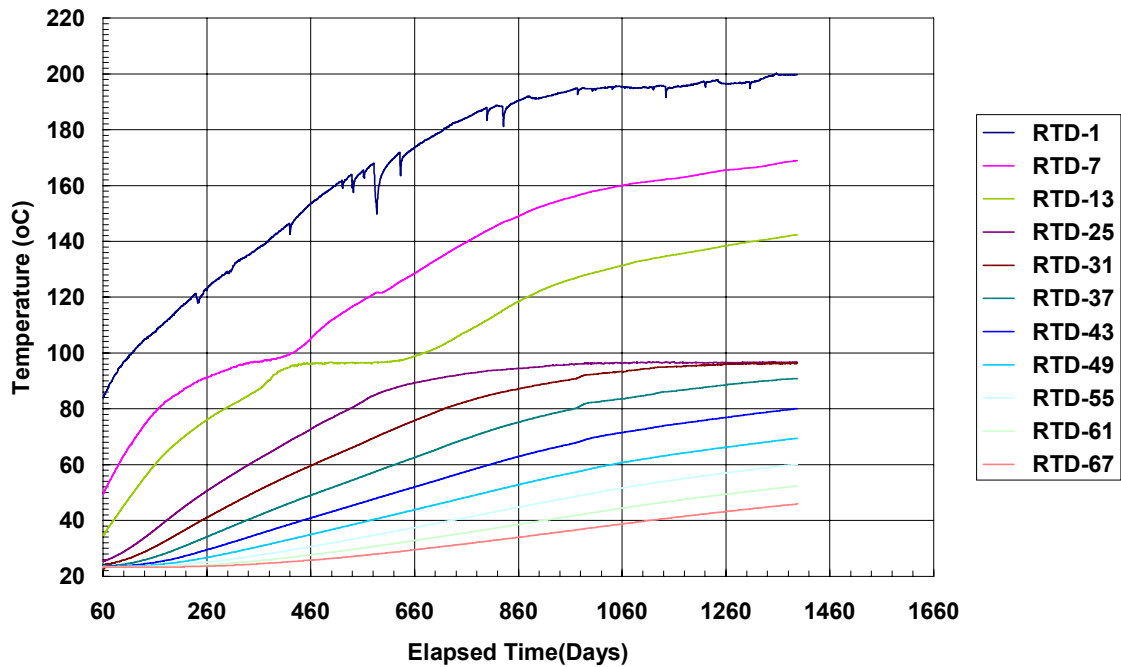


Figure 5. Temperature Evolution of Borehole 144, 12 m from Bulkhead

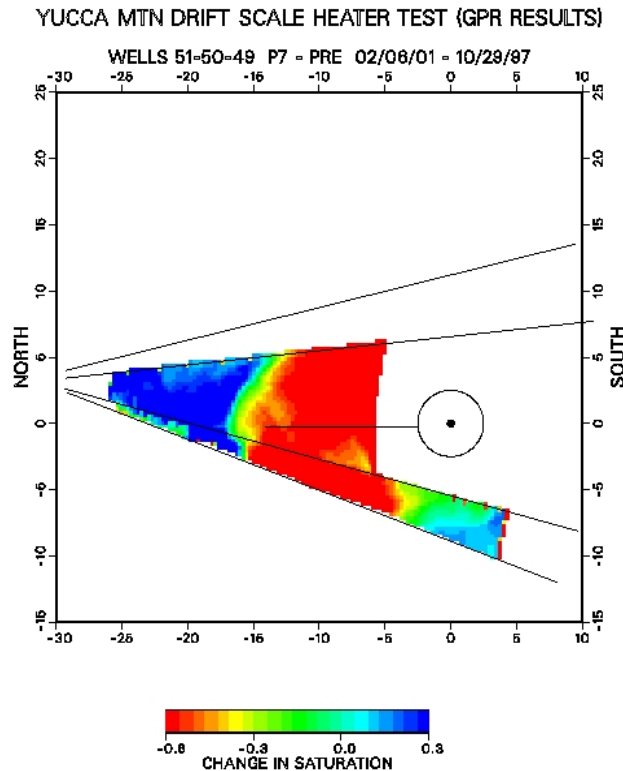
The temperature-time curves for RTD-7 to RTD-13, however, show the effect of both water movement and boiling. The length of time the temperature remains at the boiling point depends on the volume of water in this region. After the local rock mass and adjacent regions contributing water via flow have been depleted of water, the temperature rises as a result of thermal conduction alone. An extended period of nearly isothermal conditions requires water flow, since the local mass of water is insufficient to hold the temperature at the boiling point for any significant period of time (compare, for example, RTD-1 and RTD-7). Other RTDs (e.g., 19 and 25) are still at the boiling point, while RTDs beyond these (31 and higher) have not yet reached the boiling temperature. It is clear from Figure 5, however, that no significant change in the thermal evolution of this borehole has occurred. Other boreholes (not shown) show very similar behaviors, although the times when they reach or emerge from the isothermal boiling period depends on their location.

All of these recent data are very much in keeping with earlier observations. Certain boreholes show very extended periods at the boiling point of water (up to 360 days), and this may be attributed to replenishment of the water in this zone by water flow, although this phenomenon was also noted in earlier reports (Williams 2001). The extended periods of boiling may be also due to the location of the temperature sensors, since the rate of advance of the boiling front will slow with increasing radial distance from the heated drift.

### 3.1.2.2 Integrated Interpretation of Geophysical Methods of Monitoring Water Movement

The geophysical methods used to monitor the spatial distribution and the temporal variation of moisture content are GPR, ERT, and neutron logging. Water movement is inferred from the measured spatial distribution and temporal variation of the moisture content. In what follows, all of the geophysical measurements are referenced to the preheating moisture content of the rock. The results, therefore, represent changes in moisture due to the heating event.

**Ground-Penetrating Radar Results**—In general, the GPR results show drying in regions near the heaters and increasing moisture content outside of the drying regions, in general agreement with the ERT and the neutron logging results. Figure 6 shows the GPR results measured in holes 49, 50, and 51 on February 8, 2001 (day 1,161). The circle in this figure represents the heated drift. Shades of blue represent regions where water has been added, while shades of red and orange represent dryout zones.



NOTE: The circle represents the heated drift of the Drift Scale Test. Distances are given in meters from the center of the drift.

Figure 6. Ground-Penetrating Radar Results, Showing the Difference between Pretest (Oct. 29, 1997) and Feb. 8, 2001 (Day 1,161) Saturation Values

These results are very similar to those shown earlier, for example in the YMS&ER (DOE 2001a). Due to continued heating since these earlier surveys, the dryout zones have expanded slightly.

**ERT and Neutron Logging Results**—ERT is conducted in 8 planes in the Drift Scale Test: two vertical planes from the Access Observation Drift to the heated drift intersecting the heated drift at 4.6 and 25 m (15 and 82 ft) from the bulkhead, three vertically up planes parallel to the heated drift axis, and three vertically down planes parallel to the heated drift axis. As shown in *Drift Scale Test As-Built Report* (CRWMS M&O 1998), there are twelve neutron holes in the Drift Scale Test. Ten of those holes (#47 to #51, and #64 to #68) originate from the Access Observation Drift, and form two vertical arrays intersecting the heated drift at 6.4 and 26.5 m (21 and 86.9 ft) from the bulkhead, respectively. Neutron logging is also conducted in two horizontal holes parallel to the heated drift axis, at about 3.5 m (11.5 ft) above the mid-wing heater plane (holes #79 and #80). In this analysis, the ratio of the ERT and the neutron data (collected at about the same time) with respect to their preheating values are plotted in the same figure. Because the neutron logging is carried out more frequently than the ERT, neutron data obtained at about the same time as the ERT are selected to be plotted with the ERT data. In the figures that are shown, a ratio of greater than 1 means an increase in moisture content has occurred while a ratio of less than 1 indicates a loss of moisture.

Detailed images of the time progression of the drying front are given in the *Thermal Test Progress Report #6* (Williams 2001). By February 5, 2001 (day 1,158) (Figure 7), the only region where increasing moisture existed was above the heated drift at a distance greater than 25 m (80 ft) from the bulkhead.

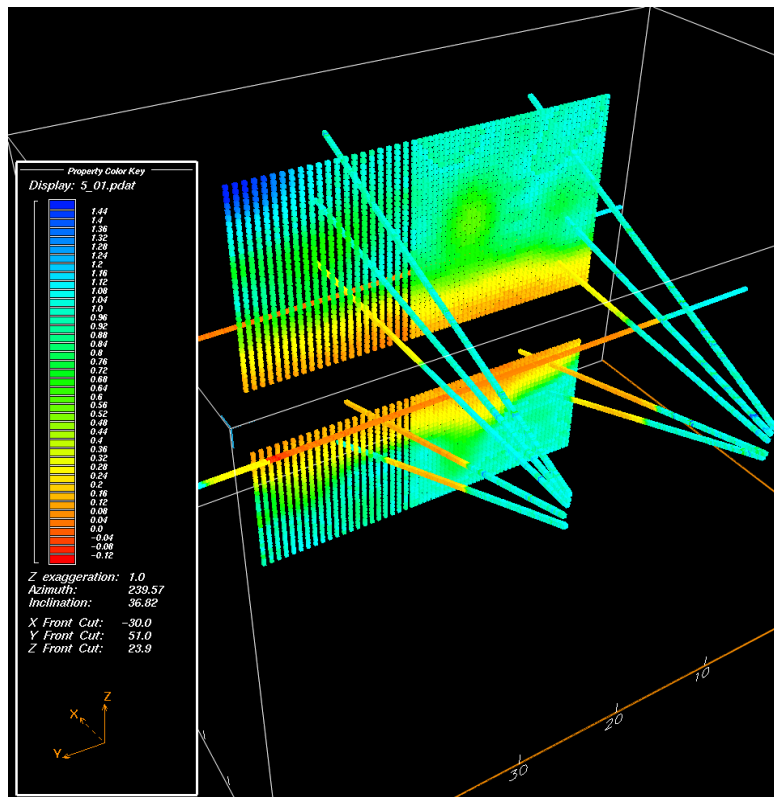


Figure 7. The ERT and Neutron Results in the Drift Scale Test  
This figure shows the ratio between the water content measurements on February 5, 2001 (Day 1,158) to that of the preheat baselines. Colored plane is a vertical slice through the Heater Drift, with the bulkhead at the right side of the drift.

### 3.1.3 Thermal-Hydrologic Model Validation—Integrated Assessment of Measurements and Comparison with Model Results

Data used for tracking thermal-hydrologic processes are the spatial and temporal evolution of (1) temperature and (2) moisture redistribution. Thermal-hydrologic coupling is reflected in temperature readings that remain at the nominal boiling temperature of  $\sim 96^{\circ}\text{C}$  ( $205^{\circ}\text{F}$ ), resulting from two-phase conditions. Periodic geophysical logging by ERT, GPR, crosshole tomography, and neutron logging are all tools for evaluating liquid saturation changes in the matrix, where the majority of liquid water resides. As fractures are mostly drained of water at ambient conditions, the fracture pore space is essentially air-filled. Periodic air permeability measurements therefore specifically target liquid saturation changes in the fractures assuming negligible thermal-mechanical effects on fracture apertures.

#### 3.1.3.1 Comparison of Measured Temperature Data with Numerical Model Predictions

Illustrations of temperature signatures that reflect thermal hydrologic coupling are presented in Figures 8a and 8b. These show the temperature profiles along the eight boreholes 137 to 144 after 39 months of heating. The plots for the measured temperatures are on the left; and the plots from simulations are on the right. For boreholes 139 and 143, both the data and simulations show a temperature plateau at nominal boiling temperature of  $\sim 96^{\circ}\text{C}$  ( $205^{\circ}\text{F}$ ) at about 15 m (49 ft) from the collar. Boreholes 139 and 143 are horizontal boreholes parallel to the wing heaters. The temperature plateau for these boreholes is a signature of drainage of condensate water just beyond the outer edge of the wing heaters. Figures 8a and 8b also indicate another set of temperature plateau at  $\sim 96^{\circ}\text{C}$  ( $205^{\circ}\text{F}$ ), located between 6 to 12 m (20 to 40 ft) from the collar of the boreholes at the heated drift. This set of temperature plateaus indicates a two-phase zone immediately outside the dryout region surrounding the heated drift. Since the volume of drying continues to increase with heating, this two-phase zone would move out and away from the heated drift with time. At 12 months of heating, this set of temperature plateau was located at around 2 to 4 m (6.5 to 13 ft) from the collar.

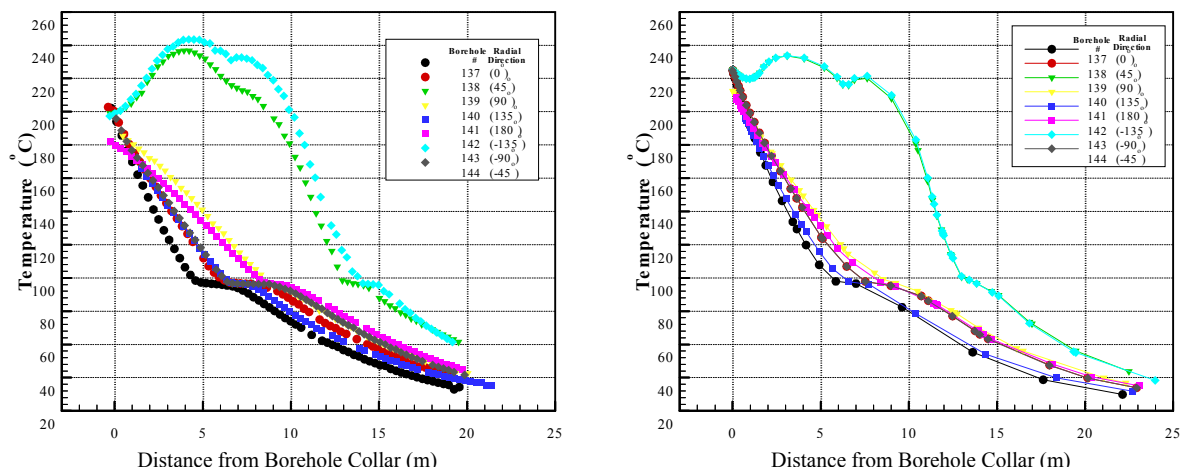


Figure 8. Measured Temperatures after 39 Months of Heating in Boreholes 137 through 144 (Left); Temperatures Predicted by Thermal-Hydrologic Model for Same Period (Right)

The data are consistent with earlier observations. In addition, the ability to model the temperature evolution indicates that it can be described quite well with the process models described in YMS&ER (DOE 2001a).

### 3.1.3.2 Air Permeability Measurements

Periodic air injection tests are performed in the twelve hydrology boreholes to assess the wetting and drying in the fractures. Wetting of fractures means increase resistance to air flow during air-injection tests, leading to a decrease in air permeability from its preheat value.

It is observed that for those borehole sections situated in zones of increased liquid saturation as indicated by other geophysical measurements (ERT, GPR, and neutron), the air permeability measurement displays a trend of decreasing permeability. As heating progresses and the drying around the heated drift and the wing heaters expands, certain borehole sections that were previously zones of increased liquid saturation would become zones of decreased liquid saturation and thus increasing air permeability.

As an illustration, the data for borehole sections 59-2 and 59-3, reproduced in Figure 9, exhibit the downward trends prior to December 1999 (about day 726). This is consistent with an increased liquid saturation in the rock. After December 1999, however, air permeability increases, which is consistent with the decreasing liquid saturations at this stage. The most recent data follow closely the trends reported earlier.

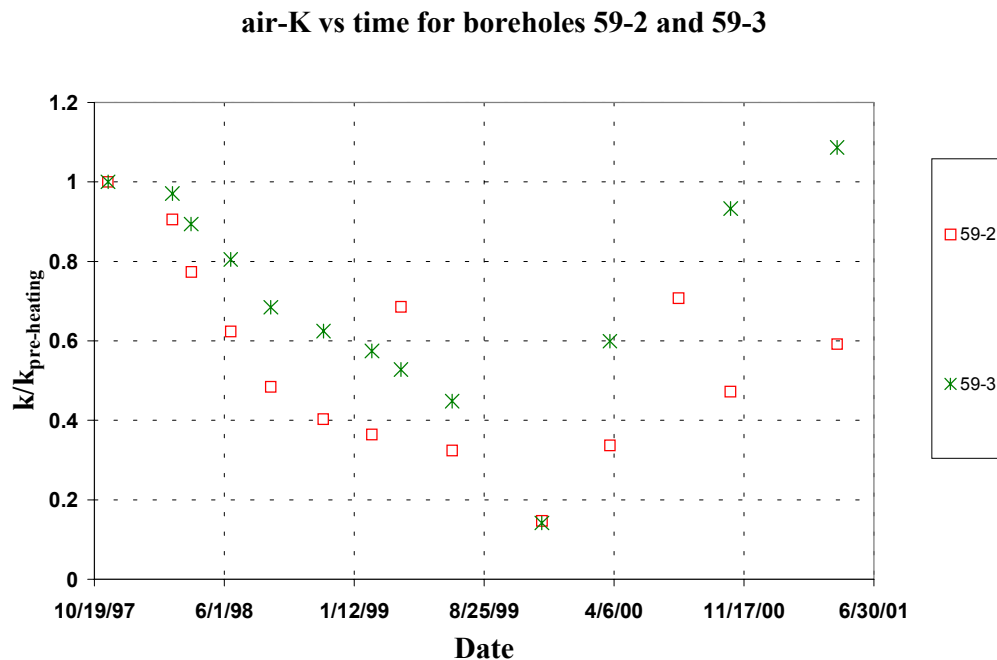


Figure 9. Measured Air Permeability (Normalized to Preheat Values) as a Function of Time for Zones 2 and 3 in Borehole 59

### 3.1.4 Thermal-Mechanical Data from the Drift Scale Test

Several tests were carried out to evaluate thermal-mechanical processes taking place in the Drift Scale Test. These include a Plate Loading Test data and an MPBX displacement test data. These data are used for performance assessment purposes in the following manner:

- Evidence of fracture deformation, either in the formation of new fractures, or in changes to existing fractures (shear slippage, aperture changes)
- Resulting changes in permeability that may affect water/vapor influx to the drift during cooling.

#### 3.1.4.1 Plate Loading Test (October 2000)

The purpose of the Plate Loading Test was to obtain rock mass elastic modulus measurements under ambient and hot conditions for the middle nonlithophysal tuff. The Plate Loading Test Niche is located about 5 m (16 ft) from the heated drift bulkhead and is driven approximately 5 m (16 ft) toward the north, perpendicular to the axis of the heated drift. The Plate Loading Test is designed to mechanically load the rock in a horizontal orientation using large square-shaped flatjacks that press against both ribs of the Plate Loading Test Niche. The pressure was increased in a stepwise fashion, with intervening periods where the pressure was reduced. This cycling of the pressure in the flatjacks can be seen in the hysteretic behavior of the rock, which relaxes at a different modulus than when it is compressed. The rock was eventually pressurized to a maximum bearing pressure ~32 MPa (4,600 psi), resulting from a maximum flatjack pressure of about 6000 psi. The temperatures in the hot and ambient sides of the test were  $T_{hot} = 58^{\circ}\text{C}$  (136°F),  $T_{ambient} = 36^{\circ}\text{C}$  (97°F).

The resulting values of rock mass modulus from the October 17, 2000 test (day 1,047), as well as from the 1998 tests, are given in Table 1. The recent test results show higher rock mass elastic modulus values than did the 1998 tests. Some of this difference may be due to the improved testing technique, but also may reflect some temperature dependence of this parameter.

Table 1. Best Estimates of Elastic Moduli from the Plate Loading Tests

| Plate Loading Test Date | Maximum Bearing Pressure (MPa) | Ambient side of Plate Loading Test Niche (GPa) | Temperature (ambient side) °C | Heated side of Plate Loading Test Niche (GPa) | Temperature (heated side) °C |
|-------------------------|--------------------------------|--|-------------------------------|---|------------------------------|
| 5/28/1998 (day 174)     | 6.4                            | 11.7   | 25                            | 26.6  | 34                           |
| 6/9/1998 (day 186)      | 11.9                           | 11.4   | 25                            | 30.2  | 34                           |
| 10/17/2000 (day 1,074)  | 31.75                          | 17.3   | 36                            | 43.0  | 58                           |

### 3.1.4.2 MPBX Displacement Data

The middle nonlithophysal tuff has exhibited behavior that is approximately elastic, especially for purposes of design. Figure 10 compares pretest predictions of displacement for MPBX-3 with the actual data. The pretest elastic model using intact rock properties gives reasonably good estimates of rock mass displacement behavior, with the exception of the behavior at Anchor 4 at about 1060 days. Anchor 4 (15 m [49 ft] from the collar) has a sudden change to its displacement curve beginning on 11/1/2000 (day 1,062), beginning a steady descent at this point. The current hypothesis regarding this event at Anchor 4 is that a major fracture between Anchors 3 and 4 is now sufficiently within the thermal pulse that it is closing.

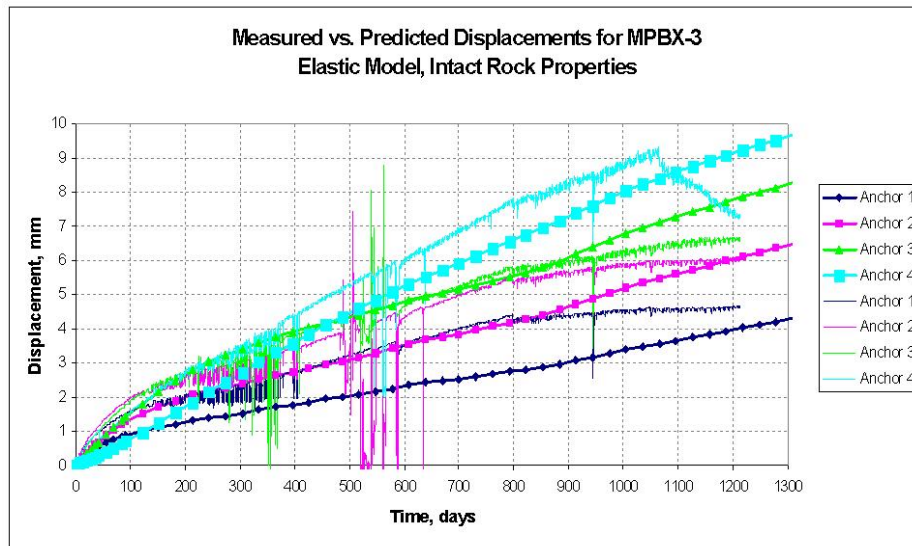


Figure 10. Measured (Lines Only ) vs. Predicted Displacements (Lines with Symbols) for MPBX-3

During boiling, oscillations developed in the MPBX displacement data, which appear to be due temperature oscillations in the borehole caused by water recirculation. It is thought, however, that the surrounding rock mass is negligibly affected by these temperature oscillations, and thus the oscillating MPBX measurements do not represent the actual rock behavior.

### 3.1.4.3 Deformation of the Rock Mass as measured by the MPBX

Strain (deformation) was calculated from the displacement data measured in the MPBX holes in the Drift Scale Test. MPBX data from various length scales were used so that the responses of the rock mass to the heating are free from the influence of the measurement length. The strain data indicate that most of the deformation is limited to a region within a few meters from the collar of each hole. The strain data show that the deformation in the region above the heaters is greater than that below the heaters and that the deformation in the region away from the Access Observation Drift is greater than that in the region toward the Access Observation Drift. Values of strain calculated using the most recent data from the various boreholes monitored provide very similar trends to those observed earlier, although some discrepancy between model results (lines only) and the data (lines with symbols) appear at late times (Figure 10).

### 3.1.5 Thermal-Hydrologic-Chemical Processes in the Drift Scale Test

Since the release of the *Yucca Mountain Science and Engineering Report* (DOE 2001a) and the *Yucca Mountain Preliminary Site Suitability Evaluation* (DOE 2001b), additional liquid and gas data have been collected. In addition, important observations on mineralogic changes in the near-field environment—apparently the result of the thermal-hydrologic-chemical system generated there—have been recorded.

#### 3.1.5.1 CO<sub>2</sub> Analyses of Gas from the Drift Scale Test

In general, it has been observed that the concentration of CO<sub>2</sub> in the gas samples collected from the Drift Scale Test increase with temperature until the boiling point (~96°C [205°F]) is reached (Figure 11). Above the boiling point, the concentrations drop off significantly. This is consistent with evolution of CO<sub>2</sub> from the dissolved inorganic carbon in the pore water during heating up to the boiling point. This is supported by a general trend towards higher  $\delta^{13}\text{C}$  values as the CO<sub>2</sub> concentrations increase, indicating a progressive loss of CO<sub>2</sub> gas (which has lower  $\delta^{13}\text{C}$  values) from the dissolved inorganic carbon (which has higher  $\delta^{13}\text{C}$  values). Once the rock passes through boiling, the pore water disappears and all the dissolved inorganic carbon originally present in the water has either been converted to CO<sub>2</sub> or precipitated as secondary carbonate minerals. Currently, most of the gas sampling intervals in the Drift Scale Test are above the boiling point of water and the CO<sub>2</sub> concentrations are low (<0.2 percent). In most of the sampling intervals that are still below boiling, the CO<sub>2</sub> concentrations are continuing to increase (the highest measured concentration in April 2001 was 7.9 percent in interval 185-2 [not shown]). These most recently observed CO<sub>2</sub> concentrations are continuing to follow previously noted trends (Figure 11). The fact that the trends can be modeled is again an indication that these trends are captured by the process models in use and described in the YMS&ER (DOE 2001a).

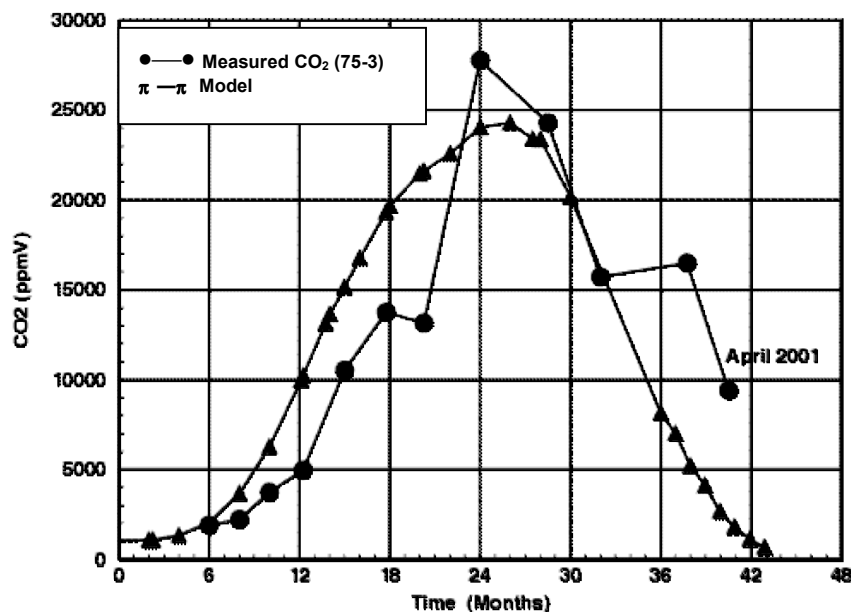


Figure 11. Evolution of Measured CO<sub>2</sub> over Time from Borehole 75, Interval 3 Compared to Drift Scale Test Thermal-Hydrologic-Chemical Model Results

### 3.1.5.2 Recent Water Analyses

Since April of 2001, eleven new water samples have been collected and analyzed, adding to the 59 collected previously from the Drift Scale test. Of the new samples, five samples represent condensates of vapor from high temperature zones in the rock above 130°C [266°F]. Four of the samples show elevated fluoride contents (above 5 ppm and as high as 66 ppm in a 171°C [340°F] sample) and all five samples show pH values below 4 (Figure 12 and Table 2). All the samples collected from zones substantially above the boiling temperature (>~96°C [206°F]) are thought to represent samples of the gas phase that are cooled in the sampling line, resulting in condensation of the water (note the temperature change from the sampled zone to the collected water). Three previously collected high temperature samples also showed similar compositions (Figure 12), indicating the phenomenon of high fluoride and low pH values from high temperature zones is not restricted only to recently collected samples. Of the nine samples collected at temperatures above 130°C [266°F] (both pre- and post-April 2001), seven show elevated fluoride contents (above 5 ppm) and five show pH values below 4. The samples also showed relatively high silica and aluminum concentrations, while Ca, Mg, and K were all below 1 ppm.

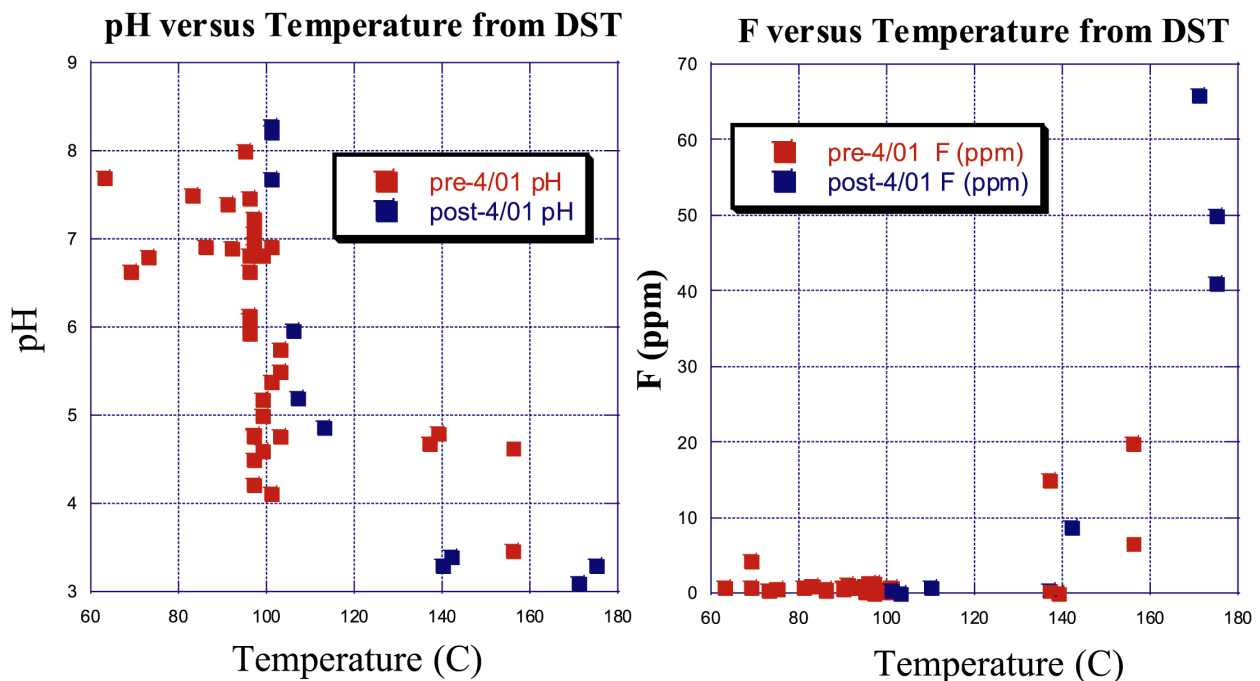


Figure 12. pH (Left) and Fluoride Concentrations (ppm) (Right) Versus Temperature in Water Samples Collected from the Drift Scale Test

Table 2. Liquid Water and Condensed Vapor Samples Collected in 2001 from the Drift Scale Test

| Date and Borehole Interval Collected | Sample Identification | Temperature of Sampled Zone (°C) | Temperature of Water Sample (°C) | Field pH | Fluoride (ppm) | Silica (ppm) | Aluminum (ppm) |
|--------------------------------------|-----------------------|----------------------------------|----------------------------------|----------|----------------|--------------|----------------|
| 4/17/01 BH 76-2                      | SPC00559464           | 101                              | 42.5                             | 7.68     | N.A.           | 42.6         | 0.33           |
| 4/17/01 BH 76-2                      | SPC00559458           | 101                              | 30                               | 8.22     | 0.38           | 44.1         | 0.34           |
| 4/17/01 BH 76-2                      | SPC00559456           | 101                              | 32.5                             | 8.29     | 0.47           | N.A.         | N.A.           |
| 4/17/01 BH 59-4                      | SPC00559466           | 107                              | 32.6                             | 5.2      | N.A.           | 1.3          | N.D.           |
| 4/17/01 BH 59-3                      | SPC00559463           | 106                              | 29.9                             | 5.96     | N.A.           | 1.2          | N.D.           |
| 4/17/01BH 59-2                       | SPC00559467           | 113                              | 32.2                             | 4.87     | N.A.           | 5.2          | 0.01           |
| 6/28/01 BH 60-3                      | SPC00559481           | 140                              | 35.0                             | 3.3      | N.A.           | 4.9          | 0.51           |
| 8/8/01 BH 60-3                       | SPC00559491           | 142                              | 56.0                             | 3.4      | 8.8            | 5.3          | 0.64           |
| 8/8/01 BH 60-2                       | SPC00559490           | 171                              | 52.0                             | 3.1      | 66             | 22.7         | 2.34           |
| 8/7/01 BH 77-3                       | SPC00559484           | 175                              | 60.0                             | 3.3      | 50             | 17.4         | 2.04           |
| 8/7/01 BH 77-2                       | SPC00559455           | 175                              | 61.0                             | 3.3      | 41             | 10.7         | 0.84           |

Samples collected from rock with temperatures below 130°C [366°F], in contrast, consistently showed pH values above 4 and fluoride concentrations below 1 ppm, no matter when they were collected (Figure 12). The condensed vapor samples showing moderate pH values (above 4) are believed to be formed by equilibration with a gas phase with high CO<sub>2</sub> concentrations. In contrast, the high fluoride samples show pH values below what can be produced by equilibration with CO<sub>2</sub> and appear to be the result of equilibration with HF (hydrogen fluoride) gas. This is borne out by calculations that show that the hydrogen ion and fluoride concentrations are present in approximately stoichiometric proportions (1:1 on a molar basis) after correction is made for complexation in the aqueous phase and minor reaction with aluminum and/or silica phases.

As noted above, the low pH values and high fluoride contents suggest equilibration with hydrogen fluoride gas. For the highest fluoride sample (66 ppm fluoride and a pH of 3.1), an HF(gas) partial pressure of 10<sup>-6.3</sup> bars is calculated if equilibration occurred at 50°C (122°F), the approximate field temperature of the collected water sample. It is important to bear in mind, however, that the concentrations of both fluoride and hydrogen ion accumulated in any aqueous phase will be a strong function of temperature. Equilibration of the gas phase with an aqueous phase at higher temperature than the sampling temperature of 50°C (122°F) will result in lower fluoride concentrations and higher pH values. For example, at 90°C (192°F), assuming the same HF fugacity, a pH of 3.88 and a fluoride concentration of 20 ppm are calculated.

The origin of the HF gas, however, is less clear. The most likely explanation for the origin of the high fluoride concentrations and low pH values is that they result from the breakdown of either Teflon used in the sampling tubes or Viton (a fluoroelastomer consisting of 66 to 77 percent fluorine) used in the packers in the boreholes. Unpublished evidence provided by Dr. Kevin Knauss (oral communication) of Lawrence Livermore National Laboratory, a researcher with 30 years of experience in conducting and analyzing hydrothermal experiments under a range of temperatures and using a wide range of materials indicates that fluoride begins to appear in hydrothermal autoclave experiments at about 150°C (302°F) when Teflon is used. Dr. Richard Metcalf of Duke Engineering conducted a telephone interview with Dave Warner

(410-392-2532; Viton Business Center, Dupont Dow Elastomers L.L.C., Elkton, MD) about potential fluoride contamination from Viton packers. During this conversation, Mr. Warner acknowledged that there was the possibility of leaching fluoride from the Viton during applications at temperatures from 177°C (350°F) and above. He also summarized a table of volatile gases output during heating, which represents gas analyses at the curing press, as the product is cured for 10 minutes at 203°C (397°F) followed by 24 hours at 111°C (232°F). In this Table, Viton E60C and Viton A released 1 percent HF(g) as a weight percent of volatile products, and Viton B released 2 percent HF(g). Although the curing of the Viton is designed to remove most of the volatile constituents of the Viton (including fluorine), it has not been established that the curing process is 100 percent effective.

A second, but less likely, possibility is that the origin of the HF gas is from interaction between vapor and fluoride-bearing minerals in the tuff (e.g., fluorite or fluorapatite). Fluorite is known to occur as a trace constituent in fractures and lithophysal cavities. At 171°C (340°F), the HF(gas) partial pressure calculated to be in equilibrium with calcite and fluorite is  $10^{-7.4}$  bars assuming a  $p\text{CO}_2$  of  $10^{-1.3}$  bars (approximately the highest observed  $\text{CO}_2$  gas concentration in the DST). This HF partial pressure is about 1 order of magnitude lower than the calculated HF partial pressure of the sample. However, when the  $p\text{CO}_2$  of  $10^{-3}$  bars measured in the borehole is used, an HF partial pressure of  $10^{-8.6}$  is calculated, more than two orders of magnitude lower. Calculations for a vapor equilibrated with both calcite and fluorite at 171°C (340°F) and allowed to cool to 50°C (122°F) without reacting with rock as it cools, predict a solution pH of about 3.7 for a  $p\text{CO}_2$  of  $10^{-1.3}$  bars. This same approach results in a predicted pH of 4.2 assuming the more applicable  $p\text{CO}_2$  of  $10^{-3}$  bars. (Similar calculations with fluorapatite in place of fluorite yield fluoride concentrations and pH values that are even further from those observed in these samples collected from high-temperature Drift Scale Test holes.) The predicted values are quite different from the observed pH of 3.1 (the pH is a log unit).

Another argument can be made that suggests that a rock origin for the HF is very unlikely. The assumption that the vapor phase is in equilibrium with fluorite is unlikely to be correct. Given that fluorite is a trace constituent of the tuff, it is very unlikely that the gas composition of the bulk vapor could be controlled by equilibrium with fluorite. Even if local equilibration were to occur, gases generated by this reaction would be diluted at a larger scale by gas generated elsewhere in the absence of fluorite, since fluorite is not ubiquitous.

### **3.1.5.3 Mineralogic Analyses of Drift Scale Test Sidewall Cores**

In November 2000, a new sidewall coring tool was used to collect sidewall cores from inclined boreholes 53 (ESF-HD-CHE-2) and 54 (ESF-HD-CHE-3) while the thermal test was in progress. Borehole intervals with visible fracturing were chosen to maximize the likelihood of finding mineral deposits resulting from water-rock interaction during the test. The locations targeted for sampling in borehole 54 were within the boiling zone as it existed in November 2000. It is important to note that these locations were part of the condensation zone above the boiling zone until the boiling zone moved outward to intersect borehole 54. Therefore, the observed test effects may be composites of condensation-zone and boiling-zone processes. Borehole 53, higher in the test block than hole 54, is still in the condensation zone and had not experienced temperatures at or above boiling at the time it was sampled.

The three samples from borehole 54, collected in two locations where the borehole intersects the boiling zone, all contain evidence of mineral deposition apparently related to the Drift Scale Test. The three products observed so far are identified tentatively using optical and scanning electron microscopy as amorphous silica, a calcium sulfate phase (gypsum or anhydrite), and a calcium-rich phase that is probably calcite. The scanning electron microscopy images in Figure 13 show one example of possible condensation-zone silica deposits, a fracture surface completely coated by terrace-like silica deposits up to a few micrometers thick. The silica deposits were apparently built up during multiple episodes of silica deposition.

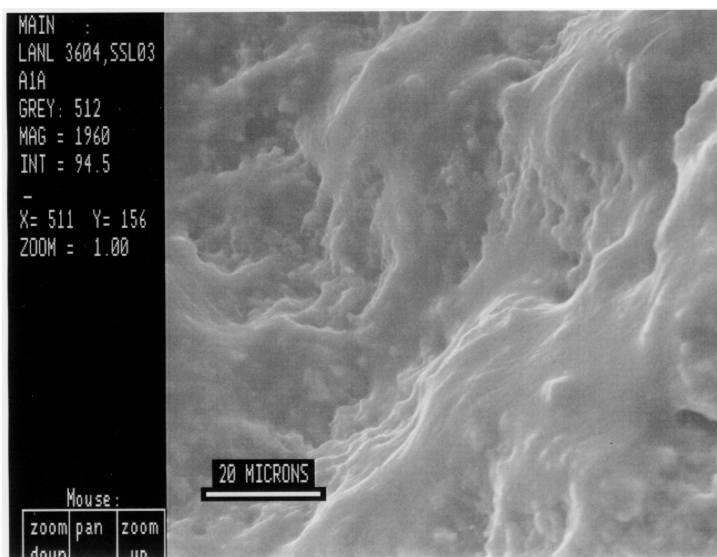


Figure 13. Terrace-Like Deposits of Amorphous Silica Coating a Fracture Surface  
Secondary-electron image.

Possible dissolution of natural fracture-coating minerals was observed adjacent to one of the thicker lobate silica deposits interpreted as condensation-zone deposits (Figure 14). A highly corroded stellerite crystal (Figure 14; pt 2) presents a strong textural contrast to the well-preserved prismatic crystal forms away from the silica deposit. Next to the corroded stellerite, a silica crystal, probably cristobalite, also appears corroded (Figure 14; pt 1). The localization of dissolution evidence close to test-related silica deposits suggests that much of the dissolved material may be redeposited after very little transport.

## 3.2 NATURAL ANALOGUE STUDIES

### 3.2.1 Introduction

Studies of natural and anthropogenic analogues are used to test and build confidence in process models. In this sense, analogues have been used to corroborate the operative processes of drift-scale flow models, as one line of evidence, among others, of the long-term operation of processes at scales too large to measure by laboratory and field-scale experiments. Analogues are also used to demonstrate that modeling codes represent the processes correctly and that they provide reasonable matches to observed data. Both qualitative and quantitative applications of natural analogues have been used by the Yucca Mountain Site Characterization Project. Examples of both types are given in this section.

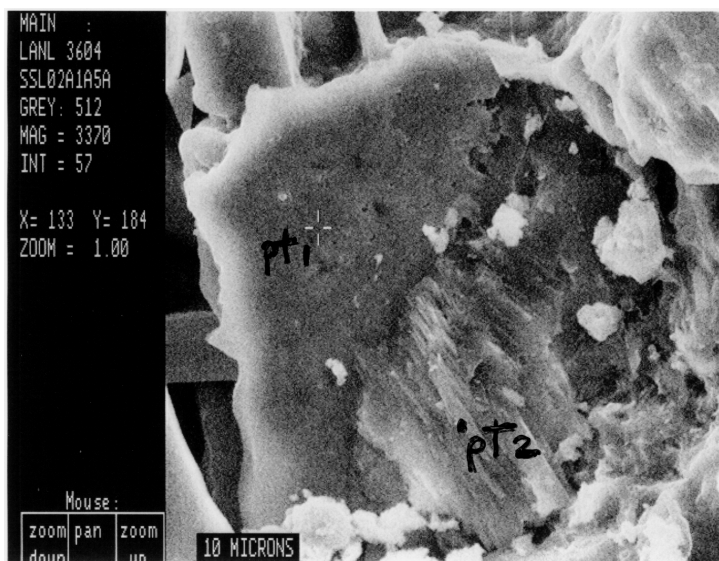


Figure 14. Corroded Pretest Crystals of Stellerite (Pt 2) and Silica (Pt 1) Formed During the Tests Secondary-electron image.

Volume 1 of *FY01 Supplemental Science and Performance Analyses* (BSC 2001b) included multiple lines of evidence for all of the thermal-hydrologic-chemical and thermal-hydrologic-mechanical processes that could affect flow paths at the drift scale. This section reflects insights from a natural analogue study of thermal-hydrologic-chemical processes at Paiute Ridge, where a detailed field investigation was followed by mineralogic analyses and modeling carried out in part since completion of *FY01 Supplemental Science and Performance Analyses* (BSC 2001b).

### 3.2.2 Paiute Ridge

The Paiute Ridge intrusive complex in partially saturated tuff at the northeast edge of the Nevada Test Site includes the Papoose Lake Sill. The sill apparently intruded into Rainer Mesa Tuff and the resulting hydrothermal process was characterized by low-temperature alteration of glass to clinoptilolite and opal.

Field observations at the Paiute Ridge intrusive complex and results from laboratory analysis of altered and unaltered tuffs provide insight into hydrothermal mineral reactions and the resulting low-temperature mineral assemblages that occur adjacent to and above the basaltic sill. The pervasive anastomosing opal veins and associated secondary minerals (e.g., clinoptilolite, calcite, cristobalite, etc.) appear to have reduced matrix or fracture permeability in the immediate vicinity of the basaltic intrusion. Hydrothermal alteration was confined to a narrow zone close to the contact zone, as indicated by major and trace element chemical data. The field investigations provide a testing ground for thermal-hydrologic-chemical computer codes and a means for validating thermodynamic and kinetic models of mineral reactions. Moreover, the widespread opal veins along fracture-matrix margins provide a means for testing and validating porosity/permeability relationships and descriptions of fracture-matrix interaction employed in thermal-hydrologic-chemical codes.

### 3.2.3 Recent Results

A one-dimensional thermal-hydrologic-chemical dual-continuum model was constructed to represent the interaction of country rock with heat released from an intrusive complex emplaced above the water table. A simplified chemical system was considered, involving precipitation and dissolution of amorphous silica. Results demonstrated the possibility of forming opal-filled veins with the source of silica derived from the matrix of the host rock. However, because of the irregularities caused by kinetic barrier effects associated with reaction of glass, general conclusions regarding mineral alteration and, specifically, the effect of heat that could be generated by a repository on tuff at Yucca Mountain cannot be drawn at this time.

## 4. IMPLICATIONS OF RECENT TEST RESULTS AND OTHER ADDITIONAL INFORMATION

### 4.1 DRIFT SCALE TEST

In Section 3 above, a number of examples of recent data have been either described or shown in graphical form. While not exhaustive, these data do show that recent test results are mostly consistent with previously collected data. The exception is in the additional water analyses collected in 2001, although even here there was some preliminary evidence that some high temperature samples showed high fluoride and low pH values in 2000. In addition, in many cases these data (thermal-hydrologic, thermal-hydrologic-mechanical, and thermal-hydrologic-chemical) have been modeled successfully, suggesting that the recent data can be understood in terms of previously developed near-field environment process models.

**Thermal-Hydrologic Results**—The data showing the greatest consistency with earlier measurements is that collected for monitoring the thermal-hydrologic system. Temperatures, liquid saturations, and air permeabilities all follow previously noted trends. These trends can be understood quite well in terms of the near-field environment thermal-hydrologic process model: continued heating causes a progressive advancement outward of the drying front. This leads to temperature increases in boreholes first up to the boiling point, and then proceeding to heat via conduction once the local water has been vaporized. Evidence also points to the local effect of vapor flow in fractures where local temperatures are higher than nearby rock and to local liquid water flow in fractures where cooling relative to nearby rock is noted. Air permeability trends are in broad agreement with geophysical measurements of bulk liquid saturations and with thermal-hydrologic modeling that predicts the partitioning of water between fracture and matrix. The general conclusion is that the additional information available has had no impact on the near-field environment thermal-hydrologic process models developed and reported in the YMS&ER (DOE 2001a).

**Thermal-Hydrologic-Mechanical Results**—Most of the thermal-hydrologic-mechanical data collected in the Drift Scale Test follow earlier results, with the exception of the most recent Plate Loading Test, indicating higher bulk elastic moduli. The additional results have no impact on drift degradation because that analysis uses independent data for rock joint properties and does not rely on bulk rock elastic modulus as an input. For thermal-hydrologic-mechanical effects, the main question concerns the effects on seepage. If thermal-hydrologic-mechanical effects (such as an increase in permeability due to shear strain) result in a permanent change in

permeability around the drift, then there is a potential effect on long-term performance. However, increases in permeability near the drift will result in lower seepage, according to the seepage model. Reductions in permeability are expected to be due to normal stresses, which do not result in permanent changes. Furthermore, the magnitude of the thermal-hydrologic-mechanical changes in permeability are smaller than the natural spatial variability of permeability.

**Thermal-Hydrologic-Chemical Results**—Analyses of CO<sub>2</sub> gas chemistry carried out recently are consistent with earlier data and can be modeled successfully with the thermal-hydrologic-chemical process model. There is no impact from these additional analyses.

New analyses of high temperature water vapor, however, show high fluoride and low pH values, which could have an impact, depending on the origin of these effects. The high fluoride and low pH contents of high temperature vapor condensates (only observed above 130°C [266°F] and most prevalent at the highest in situ temperatures of 170°C [340°F]) appear to be due to dissolution of HF (hydrogen fluoride) gas in small amounts of water condensate, followed by some reaction with aluminum and silica bearing solid or colloidal phases. There are two possibilities for the origin of this HF gas in the high temperature samples. The most probable origin is that the HF is derived from the breakdown of either Viton (a fluoroelastomer consisting of 66 to 77 percent fluorine) used in packers or Teflon used in sampling lines. The less likely alternative is that HF is generated from gas reaction with tuff containing fluorite or other fluoride-bearing phases. A rock origin is considered very unlikely for a number of reasons. First, calculations indicate that gas reactions with fluorite and subsequent condensation of that gas will not produce pH values low enough or fluoride concentrations high enough to account for the recent data collected from the high temperature boreholes. The fact that equilibration with fluorite is expected to be only a local effect given the trace concentrations of this phase in the tuff, it is likely that dilution would reduce HF partial pressures further, making a rock origin even less likely. Finally, even if a rock origin could be shown to be the case, the high temperatures needed to produce the HF and the trace concentrations of fluorite in the rock suggest that any HF gas flux would be limited in time. The duration of the high-temperatures needed is limited and the system cannot sustain high HF concentrations in the gas without depleting the available fluoride in the rock.

If the HF gas is derived from breakdown of either Viton or Teflon used in the sampling apparatus, as appears likely, then there would be no impact on the near-field geochemistry as long as this material was excluded from the eventual repository design. Since the breakdown of Viton or Teflon is considered the much more likely origin for the HF gas condensing in high temperature samples, it is likely that there will be no impact from these additional data.

Current Project efforts are focused on determining the actual source of this fluoride solution. As indicated earlier, it is considered likely to be an experimental artifact. To confirm this, some sampling will be conducted in existing “blank” boreholes that are at similar high temperatures to determine if this solution is present. The boreholes will then be filled with Viton and Teflon and additional samples taken. This sampling is to be completed by mid-December 2001.

New and extensive mineralogic analyses demonstrate that amorphous silica is the dominant secondary precipitate, consistent with the understanding developed from earlier tests and

modeling. What is not clear at this point, however, is whether the bulk of the silica forms in the condensate zone, or whether it develops due to boiling. Other secondary (newly precipitated) minerals found include calcium sulfate and calcite, both of which are expected to form in the boiling zone. The volume of all of these phases appears to be too small to have a significant impact on the fracture permeability over the time scales of the repository.

## 4.2 IMPLICATIONS OF NATURAL ANALOGUE STUDIES

The Paiute Ridge study included detailed field observations of mineralogically-induced changes to permeability caused by heat accompanied by thermal-hydrologic-chemical modeling to determine the origin of the silica filling fractures at this site. Preliminary modeling results suggest that the silica could be locally derived from rock matrix. The implications of results from this study still need to be related to thermal-hydrologic-chemical models developed for Yucca Mountain in order to make a clear statement on their impact.

## 5. REFERENCES

AP-2.14Q, REV 2, ICN 0. *Review of Technical Products and Data*. Washington, D.C.: U.S. Department of Energy, Office of Civilian Radioactive Waste Management. ACC: MOL.20010801.0316.

AP-SIII.1Q, Rev. 0, ICN 1. *Scientific Notebooks*. Washington, D.C.: U.S. Department of Energy, Office of Civilian Radioactive Waste Management. ACC: MOL.20000516.0002.

BSC (Bechtel SAIC Company) 2001a. *Drift-Scale Coupled Processes (DST and THC Seepage) Models*. MDL-NBS-HS-000001 REV 01 ICN 01. Las Vegas, Nevada: Bechtel SAIC Company. ACC: MOL.20010418.0010.

BSC 2001b. *FY01 Supplemental Science and Performance Analyses, Volume 1: Scientific Bases and Analyses*. TDR-MGR-MD-000007 REV 00 ICN 01. Las Vegas, Nevada: Bechtel SAIC Company. ACC: MOL.20010801.0404; MOL.20010712.0062; MOL. 20010815.0001.

CRWMS M&O (Civilian Radioactive Waste Management System Management and Operating Contractor) 1998. *Drift Scale Test As-Built Report*. BAB000000-01717-5700-00003 REV 01. Las Vegas, Nevada: CRWMS M&O. ACC: MOL.19990107.0223.

CRWMS M&O 1999. *Single Heater Test Final Report*. BAB000000-01717-5700-00005 REV 00 ICN 1. Las Vegas, Nevada: CRWMS M&O. ACC: MOL.20000103.0634.

CRWMS M&O 2000a. *Near Field Environment Process Model Report*. TDR-NBS-MD-000001 REV 00 ICN 03. Las Vegas, Nevada: CRWMS M&O. ACC: MOL.20001121.0041.

CRWMS M&O 2000b. *Multiscale Thermohydrologic Model*. ANL-EBS-MD-000049 REV 00 ICN 01. Las Vegas, Nevada: CRWMS M&O. ACC: MOL.20001208.0062.

DOE (U.S. Department of Energy) 2001a. *Yucca Mountain Science and Engineering Report*. DOE/RW-0539. Washington, D.C.: U.S. Department of Energy, Office of Civilian Radioactive Waste Management. ACC: MOL.20010524.0272.

DOE 2001b. *Yucca Mountain Preliminary Site Suitability Evaluation*. DOE/RW-0540. Washington, D.C.: U.S. Department of Energy, Office of Civilian Radioactive Waste Management. ACC: MOL.20011101.0082.

Williams, N.H. 2001. "Contract #: DE-AC08-01NV12101—Thermal Test Progress Report #6." Letter from N.H. Williams (BSC) to S.P. Mellington (DOE/YMSCO), April 19, 2001, PROJ.04/01.030, with enclosure. ACC: MOL.20010612.0531.

INTENTIONALLY LEFT BLANK